Available online at www.sciencedirect.com
ScienceDirect
Organic Geochemistry 39 (2008) 188–202
Organic Geochemistry
www.elsevier.com/locate/orggeochem

In situ imaging of organic sulfur in 700–800 My-old Neoproterozoic microfossils using X-ray spectromicroscopy at the S K-edge

Laurence Lemelle [a,b], Philippe Labrot [c], Murielle Salomé [d], Alexandre Simionovici [e], Michel Viso [f], Frances Westall [c,*]

[a] *Université de Lyon, Ecole Normale Supérieure de Lyon, France*
[b] *CNRS, UMR5570, USR3010, France*
[c] *Centre de Biophysique Moléculaire, CNRS, Rue Charles Sadron, 45071 Orléans Cedex 2, France*
[d] *ID21 Beamline, European Synchrotron Radiation Facility (ESRF), 6 rue J. Horowitz, BP 220, 38043 Grenoble Cedex, France*
[e] *LGIT, Observatoire des Sciences de l'Univers de Grenoble, BP 53, 38041 Grenoble Cedex, France*
[f] *CNES, 2 place Maurice-Quentin, 75039 Paris Cedex 01, France*

Received 26 March 2007; received in revised form 26 September 2007; accepted 30 October 2007
Available online 21 November 2007

Abstract

The study of very ancient microfossils has recently raised contentious issues regarding interpretation of the biogenicity of the structures. In situ investigation of certain elements such as sulfur within potential microfossils is a powerful complement to other methods of investigation that can provide valuable information on biogenicity. We present here a first such study on Precambrian microfossils from the 700–800-My-old Neoproterozoic Draken Formation, Svalbard, using scanning X-ray microscopy (SXM) in the fluorescence mode and X-ray absorption near edge spectroscopy (XANES) at the sulfur K-edge. SXM allowed mapping of up to 300 ppm of probably endogenous sulfur within the kerogenous walls of *Myxococcoides chlorelloidea* microfossils. XANES showed that the sulfur is most likely contained in heterocyclic organic compounds, such as thiophene(s).

1. Introduction

The identification and study of microfossils in Precambrian sedimentary rocks is still challenging, despite its importance in the resolution of critical scientific issues such as reliably establishing the appearance of life on Earth and the onset of different biogeochemical cycles. One of the major difficulties results from the very small size of the structures (μm to sub-μm) and the difficulty in correlating the morphological and biochemical characteristics of such minute fossils (Buick, 1990; Schopf, 1993; Brasier et al., 2002; Schopf et al., 2002). Since it is principally the wall or sheath of the microorganism that is preserved (Knoll, 1982; Westall, 1997), only a very tiny fraction of the chemical information present in the original cell has the potential of being partly transformed into kerogen during diagenesis.

* Corresponding author. Tel.: +33 (0)2 38 25 79 12; fax: +33 (0)2 38 63 15 17.
E-mail address: westall@cnrs-orleans.fr (F. Westall).

0146-6380/$ - see front matter © 2007 Elsevier Ltd. All rights reserved.
doi:10.1016/j.orggeochem.2007.10.008

Whereas whole rock analysis of Precambrian rocks provides bulk information on the totality of the carbonaceous material in a sample, including the allochthonous and reworked organic fractions, in situ analysis at the micron scale is required to obtain specific information on a given microfossil and to detect any elemental, molecular or isotopic differences in the microfossil population.

Over the last few years, significant advances have been made in obtaining in situ carbon data on individual Precambrian fossilized cells, for example, micro-isotopic measurements made on the walls of large microfossils with an ion microprobe (House et al., 2000), μm -scale carbon mapping with an electron microprobe (Boyce et al., 2001), as well as in situ organic analysis with laser micropyrolysis gas chromatography–mass spectrometry (GC–MS; Arouri et al., 2000), laser Raman microspectroscopy (Arouri et al., 2000; Schopf et al., 2002), Fourier transform infrared spectroscopy (FTIR; Marshall et al., 2005) and C-XANES (X-ray near edge spectroscopy of carbon). C-XANES has already been successfully used in the analysis and imaging of fossil material such as permineralized plant fossils of Devonian age (Boyce et al., 2002) or coal (Cody et al., 1996). In this study, we show that the in situ characterisation of sulfur using XANES at the K-edge can lead to novel and complementary results. S K-edge XANES was first shown to be an efficient probe for S-containing metabolites in intact biological systems on human blood (Pickering et al., 1998; Rompel et al., 1998).

Compared to carbon, little in situ work on sulfur at the micron scale has been done, although sulfur is the fifth most abundant element in planktonic cells and the third most abundant in sedimentary organic matter (OM; Tissot and Welte, 1984). Whereas living biomass generally contains between 0.5% and 1.5% sulfur, kerogen derived from marine OM may contain up to 10% owing to the adsorption of allochthonous S to the kerogen (Summons, 1993). The important role of sulfur in the formation and preservation of fossil sulfur-rich OM was established on the basis of analysis of organic extracts from whole rocks (Durand and Monin, 1980; Whelan and Thompson-Rizer, 1993). By forming intermolecular sulfur bonding (single, double or polysulfide links) and sequestering organic material inside a macromolecular network, sulfur stabilizes labile compounds such as lipids, thereby prolonging their lifetime in the geological record (e.g., Kohnen et al., 1990). Advances in macroscopic S L-edge XANES and, to a lesser extent, S K-edge XANES methods offer a way of directly investigating the organically bound and inorganic sulfur forms in complex fossilized organic material. These methods have been applied to describe maturation vs. S speciation in sulfur-rich kerogen, asphaltenes, petroleum, coals and oil shales (see Fleet, 2005; Kelemen et al., 2007 for a review of applications). In particular, S K-edge XANES studies (Sarret et al., 1999) showed that, with increasing alteration, the proportion of disulfide and sulfide species decreases in asphaltene, whereas that of the most oxidized sulfur species increases. They also demonstrated that, regardless of kerogen type, the ratio of aliphatic to total organic sulfur decreased concomittantly with aromatic carbon as the level of maturity increased (Kelemen et al., 2007). In general, the intimate coexistence of minute amounts of organic, and major amounts of inorganic, sulfur species dispersed in the mineral matrix (Whelan and Thompson-Rizer, 1993; Acholla and Orr, 1993) implies that in situ studies, at a sub-micron scale, are even more critical for sulfur than for carbon. A few studies using in situ elemental imaging of sulfur have been performed on 100 μm sized, well preserved permineralized wood cells using an electron microprobe (Boyce et al., 2001). The correlation between the elementary C and S maps suggested that sulfur had been incorporated into organic compounds and it was proposed that the in situ S/C ratio could provide an indication of the types of cell wall compounds originally present in the living cell (Boyce et al., 2001). A first attempt at in situ elemental imaging of Precambrian cells was also made using secondary ion mass spectrometry (nanoSIMS), showing uncorrelated C, N and S distributions (Oehler et al., 2006). The in situ determination of the amount and speciation of sulfur on an organic-walled microfossil therefore appears to be a promising approach for obtaining information about the state of preservation of its residual OM and about the original cell wall compounds.

In this study, our goal was to detect and quantitatively characterise the sulfur distribution and speciation, if any, in the carbonaceous wall of individual Precambrian microfossils (*Myxococcoides chlorelloidea*) from the 700–800 My-old Draken Formation on Spitzbergen. Given the small amount of S and the micron-scale thickness of the microbial walls, one of the most promising techniques for achieving this goal is the combination of in situ X-ray fluorescence microscopy with X-ray absorption

near edge spectroscopy (XANES) at the sulfur K-edge using a micro-focussed synchrotron X-ray beam (Susini et al., 2002; Prietzel et al., 2003). Qualitative scanning X-ray microscopy (SXM) has been applied to search for S bound to organic molecules (thiol and alkyl monosulfide) in recent, single prokaryotic cells (Lemelle et al., 2003). In that study, an *Escherichia coli* cell was imaged as a micron-sized rod containing more phosphorus than S, with a XANES spectrum characterized by a strong peak attributed to the absorption edge of an amino acid-linked S species. The same technique permitted imaging of the distribution of structures interpreted as probable terrestrial microorganisms that contaminated the surface of the Tatahouine meteorite (Lemelle et al., 2004). Using the same methodology, amino acids were detected in SiO_2 filaments from fossil hydrothermal chimneys a few thousand years old (Foriel et al., 2004). Our SXM study at the S K-edge of 700–800 My-old microfossils differs from earlier studies in that the refractory macromolecular organic complex has undergone diagenesis and hundreds of millions of years of post-diagenetic alteration, processes inducing critical changes in the mineral and organic phases that are eventually responsible for the difficulties in the recognition of very ancient and/or metamorphosed Precambrian microfossils (Buick, 1990).

2. Materials and methods

2.1. Sample and preparation

2.1.1. Draken Formation microfossils

The microfossils come from the well characterized 700–800 My-old Draken Formation on Spitsbergen, a conglomerate formed in a tropical tidal flat/lagoonal setting (Knoll, 1982; Knoll et al., 1991). The mainly dolomitic conglomerate contains siliceous clasts formed in situ within the sediment. The formation contains some 28 different species of microfossils (Knoll, 1982; Knoll et al., 1991), representing both components of local microbial mats as well as allochthonous photosynthetic planktonic cells washed into the depositional area. We chose the vesicle-like microfossil Myxococcoides, described by Knoll (1982) and Knoll et al. (1991) as probably belonging to a planktonic photosynthetic species of unidentified affinity (either prokaryotic cyanobacterial or eukaryotic algal). These well preserved microfossils occur either isolated or in groups in both the silicified microbial mats and the dolomicrite clasts. The ca. 20 μm diameter cells we studied occur in redeposited cherty clasts in the conglomerate (Figs. 1A, 2A and 4A) and are characterized by a conspicuous, 1–2 μm thick, dark brown wall in light microscope thin section observation. Occasionally, they contain round internal vesicles and sometimes an eccentric internal wrinkled bleb. Small pyrite crystals (many having a framboidal habit) are associated with the microfossils in the silicified clasts. The carbon isotope signal of −28‰ is typical for photosynthetic fractionation, whereas the sulfur isotopes, measured on the associated pyrite crystals, reflect sulfate reduction (Knoll, 2003).

2.1.2. Petrological section preparation

A set of polished, 30 μm thick sections were prepared from the fossiliferous conglomerate. Sections containing silicified clasts, which contain the best preserved microstructures, were studied. Pre-selection of the microfossils was made with a petrographic microscope (transmitted and reflected light, Olympus BX51) and the selected microfossils were carefully characterized using optical microscopy. Two clasts containing microfossils identified as *Myxococcoides chlorelloidea* by Knoll (1982) and Knoll et al. (1991) were selected for study. A circle was engraved around each microfossil on the surface of the polished sections for location purposes, using a special objective equipped with a diamond tip (Leica M25). The sections were gently etched in S-free HF (1%, 40 min) to remove a few tens of nm of the surface, as well as laboratory surface contaminants. The etched sections were carefully washed with ultra-pure water in multiple baths for 5 h and finally dried in a vacuum chamber. Non-etched thin sections were also analyzed to verify that the etching did not introduce artifacts or contaminate the fossil OM. The presence of organic carbon in *Myxococcoides chlorelloidea* cells (exhibiting a brownish color in light microscopy) was confirmed using micro-Raman spectrometry and EDX with a scanning electronic microscope (SEM; Labrot, 2006). To aid location and detect surface contamination, the selected microfossils were scanned with an atomic force microscope (Nanoscope IIIa, D3100 Digital Instruments). A part of the fossiliferous thin section was Pt coated and imaged using SEMs equipped with an energy dispersive X-ray spectrometer (Hitachi S4200/S4500 FEG-SEM at the University of Orléans and ZEISS DSM 982 Gemini at the Faculty of Medicine, University of Tours). A 1 cm^2 section of the petrographical

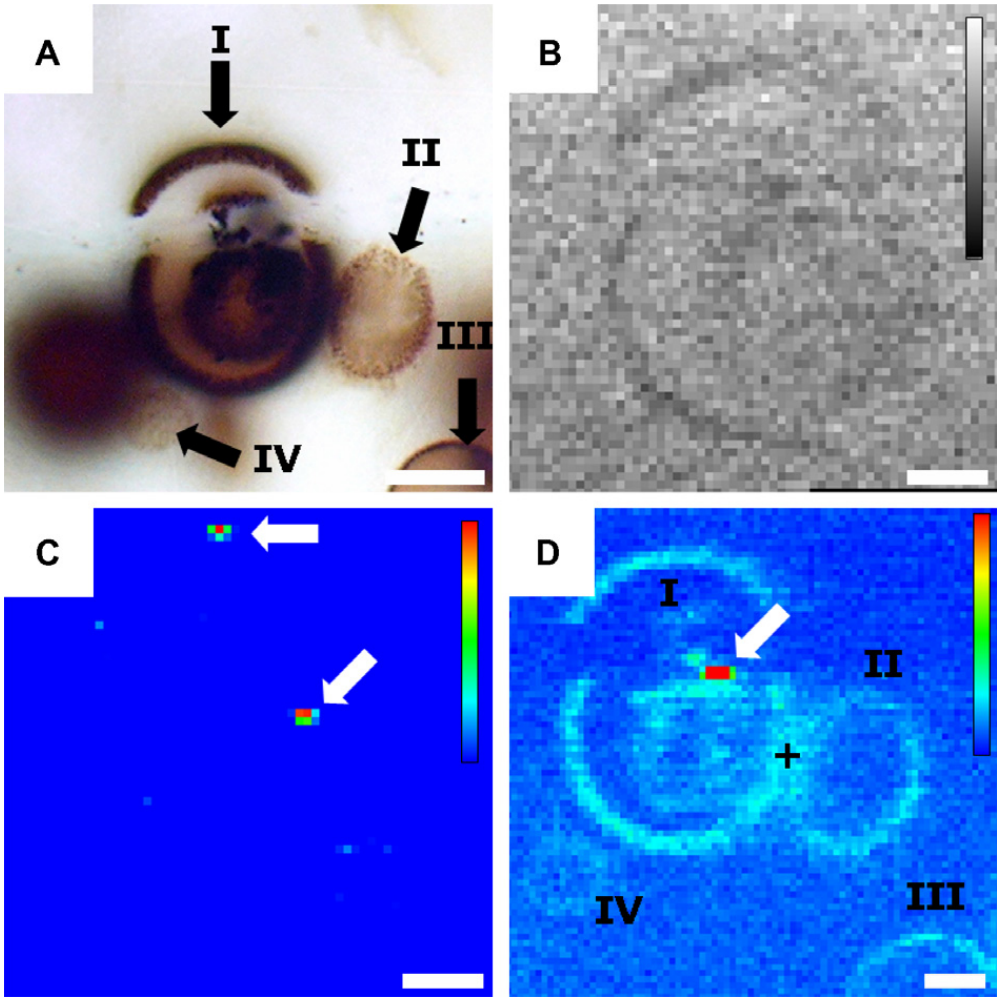

Fig. 1. Cluster of *Myxococcoides* in 700–800 My-old Draken conglomerate from Svalbard. (A) Optical microscope image in transmitted light of a cluster truncated at the surface of the thin section. The main cell (I) located in the centre of the image, 23.5 μm in diameter, is *Myxococcoides chlorelloidea* (Knoll, 1982; Knoll et al., 1991). The organic wall has been disrupted by a vein filled with secondary quartz. This cell has an internal vesicle and is flanked by other cells, II–IV; scale bar 10 μm. (B) Fluorescence map obtained at 2.5 keV of Si distribution showing depletion corresponding to the carbon rich wall of microfossil (I); scale bar 5 μm. (C) Fluorescence map obtained at 7.2 keV, integration time 3 s per pixel, showing distribution of Fe, located only in pyrite crystals (white arrows); scale bar 5 μm. (D) Fluorescence map obtained at 2.5 keV, integration time 3 s per pixel, showing distribution of S in both pyrite crystal and organic wall of microfossils I–IV. White arrow indicates lower pyrite crystal in image C. Black cross indicates area selected for S K-edge micro-XANES analysis; scale bar 5 μm.

section enclosing the microfossils was cut from the non-Pt coated portions of the fossiliferous thin sections for focussed ion beam sectioning (FIB).

2.1.3. FIB section preparation

A section normal to the cell wall of a *Myxococcoides chlorelloidea* was made with a 20 keV Ga Philips FIB 200 TEM instrument at the Centre Pluridisciplinaire de Microscopie Electronique et de Microanalyse at the University of Marseille. The thin sections were coated with a thin layer of Au (4 nm) to permit secondary electron imaging and to avoid charging at the surface caused by the ion beam. The microfossils were located using the circles made with the diamond tip and the AFM images. A 1 μm Pt layer was deposited on top of the section surface in order to protect it from Ga^+ sputtering damage. The sectioning process by sputtering was monitored using secondary electron imaging. The 100 nm ultra-thin section was deposited on to a carbon film-coated, 3 mm diameter Cu-TEM grid using a micromanipulator.

2.2. Analytical procedure

2.2.1. SXM set-up

With a 2–7 keV energy range, the ID21 scanning X-ray microscope (SXM) of the European Synchro-

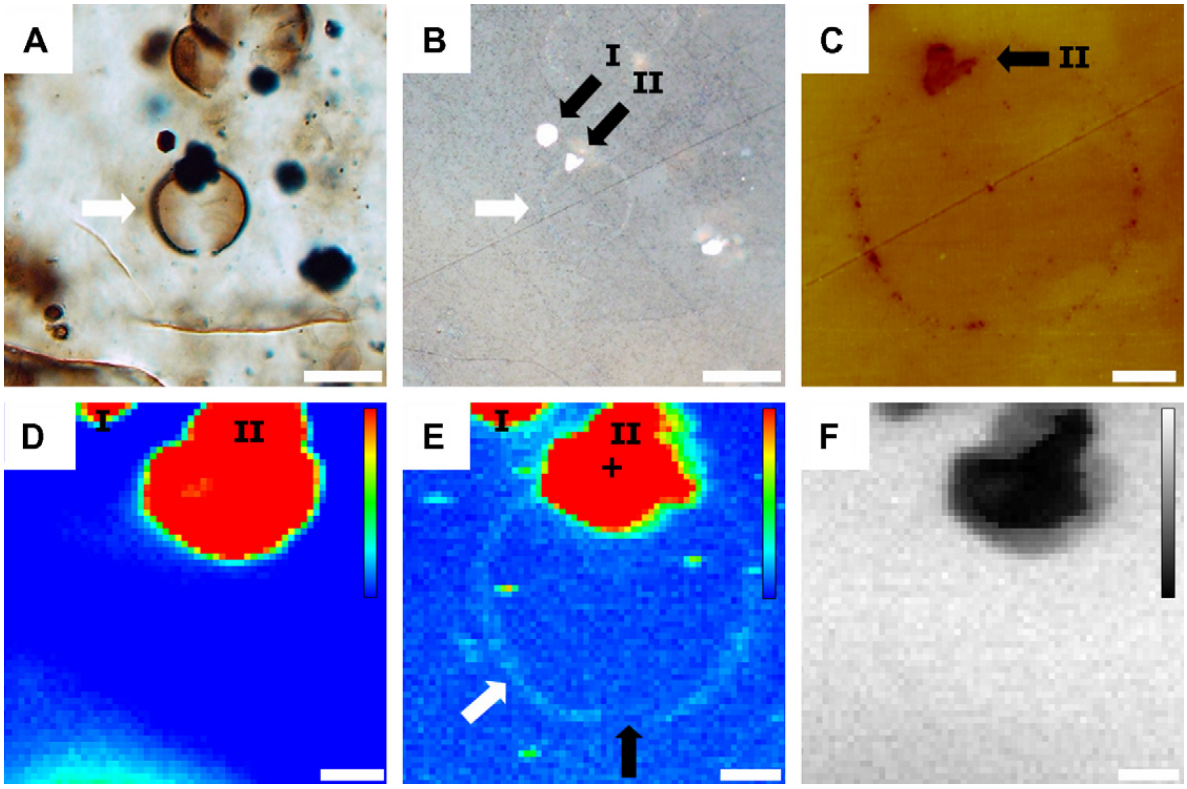

Fig. 2. *Myxococcoides chlorelloidea* cell in Draken conglomerate. (A) Optical microscope image in transmitted light of a 24 μm *Myxococcoides chlorelloidea* cell (white arrow). Note the black pyrite crystals associated with organic wall and in adjacent matrix, as well as interruption of wall in the bottom; scale bar 20 μm. (B) Same fossil (white arrow) in reflected light showing position of two pyrite crystals (I and II, black arrows); scale bar 20 μm. (C) AFM image in contact mode of cell in (A) exposed at upper surface of polished thin section. Black arrow points to pyrite crystal II; scale bar 5 μm. (D) Fluorescence map obtained at 7.2 keV, integration time 4 s per pixel, showing distribution of Fe, located only in pyrite crystals I and II; scale bar 5 μm. (E) Fluorescence map obtained at 2.5 keV, integration time 3 s per pixel, showing distribution of S in both pyrite crystal and organic wall (white arrow). Note the absence of S in the area indicated by a black arrow, which corresponds to interruption of organic wall. Black cross indicates area selected for S K-edge XANES analysis; scale bar 5 μm. (F) Fluorescence map obtained at 2.5 keV showing distribution of Si and depletion corresponding to pyrite grain and carbon rich wall; scale bar 5 μm.

tron Radiation Facility (ESRF) in Grenoble (Susini et al., 2002) is a unique tool for microspectroscopy at the sulfur K-edge, attaining high spatial (0.5 μm) and spectral (0.25 eV) resolution. It was operated at around 2472 eV, close to the sulfur K-edge. The harmonics rejection was ensured by a set of two parallel silicon mirrors deflecting in the horizontal plane with an incident angle of 8 mrad. The energy scan was performed with a fixed exit, double crystal Si(1 1 1) monochromator providing a spectral resolution of 0.25 eV in this configuration. A tantalum Fresnel zone plate lens was used for focussing, demagnifying the X-ray source to generate a 0.5×0.3 μm spot (horizontal × vertical) with a photon flux of 4×10^8 photon s^{-1}. Microfluorescence maps were also obtained at the Fe K-edge at around 7112 eV with a comparable set up.

The sample was positioned at an angle of 60° (90° between beam and fluorescence detector axis) with respect to the incoming beam. It was mounted on a mechanical sample stage combining a stepper motor equipped stage (10×10 mm^2) for coarse sample positioning and a piezoelectric stage (100×100 μm^2) for accurate scanning of the selected area. The selected clasts in the 30 μm thick petrographical sections were centered in the hole of a high purity plastic sample holder (Peek, free of Fe and S traces). The FIB cuts mounted on TEM grids were held between 4 μm thick Ultralene foils. Prealignment of every sample was ensured using the light video-microscope located inside the X-ray microscope chamber.

2.2.2. Fluorescence imaging and XANES at the ID21 beamline

Elemental composition maps were obtained by raster scanning of the sample in order to acquire a two-dimensional (2D) image point-by-point. The

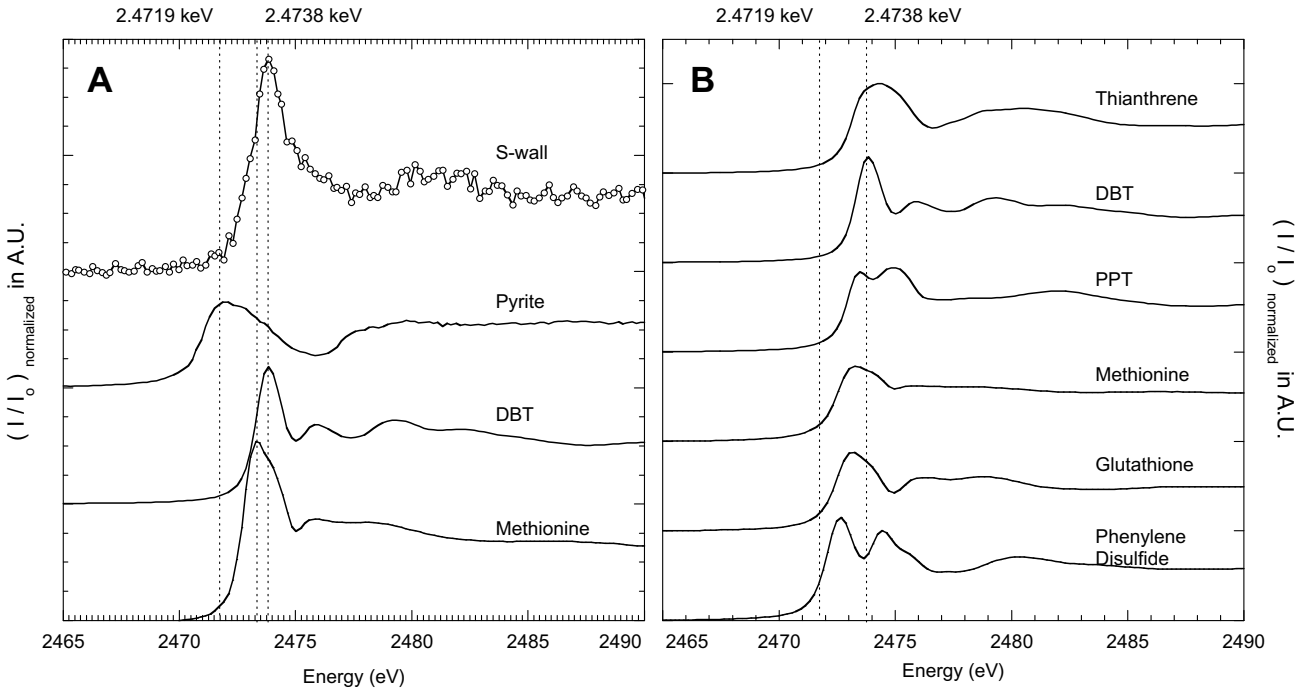

Fig. 3. Micro-XANES sulfur K-edge spectra obtained from pyrite crystal II in Fig. 2(E) associated with *Myxococcoides chlorelloidea* cell wall and from the junction of two spherical cells in Fig. 1(D) (S-wall). Energy corresponding to white line peak of organic S compound is 2473.8 eV, a 2 eV difference vs. inorganic sulfide (pyrite grain), the main form of S in the sample. Comparison with standards (Fig. 3b) shows most likely candidate for organic S to be heterocyclic sulfide (dibenzothiophene, DBT).

fluorescence photons emitted by the sample were collected with an energy-dispersive high purity Ge detector (Princeton Gamma-Tech) with an energy resolution FWHM of 135 eV (Mn Kα line), mounted in the horizontal plane at 90° to the beam. This geometry minimizes the inelastic scattering contribution to the fluorescence spectrum, which may decrease the signal/noise ratio. In order to detect fluorescence from low Z elements, the microscope was operated under vacuum. The count rate was kept below 5000 counts s^{-1}. For each pixel of the image, a full fluorescence spectrum was recorded, allowing off line reconstruction of maps for several elements in the sample. Mapping was recorded with incident beam energy of 7 keV and 2.5 keV respectively. Before mapping at high spatial resolution and high counting rate (steps of 0.5–2 μm, counting time of 2–5 s), mapping at low resolution and low counting rate (steps of 5 μm, counting time of 300 ms) was performed to select the most suitable cell in the 100 μm × 100 μm scanned areas.

For semi-quantitative S analysis, a 3-mm thick multi-element reference target (silica-rich glass SRM 620 standard from the NIST) was used as the matrix compositional reference material. SO_3 concentration was 0.28 wt%, with an uncertainty of 0.02 wt%. The glass had the following composition: SiO_2 72.08 ± 0.08, Na_2O 14.39 ± 0.06, CaO 7.11 ± 0.05, MgO 3.69 ± 0.05, Al_2O_3 1.8 ± 0.03, K_2O 0.41 ± 0.03, SO_3 0.28 ± 0.02, As_2O_3 0.056 ± 0.003, Fe_2O_3 0.043 ± 0.004, TiO_2 0.018 ± 0.002 wt%. The spectra were processed with a non-linear least squares fitting software, PyMca, developed at the ESRF: (http://www.esrf.fr/computing/bliss/downloads/index.html#PyMca) for subtracting the background and calculating the Kα net peak areas. The net peaks were converted to intensity by normalizing with the incident beam intensity. Characteristic spectra for the cell wall and surrounding matrix were obtained by either averaging the few spectra collected on positions selected after mapping the cell, or by off-line averaging of the spectra of interest from a reconstructed map with the ESRF Artemis software (http://www.esrf.fr/computing/bliss/downloads/index.html#Artemis).

For S speciation, the energy was scanned between 2450 eV and 2530 eV in 0.2 eV energy steps and 1s dwell time. The ID21 SXM was first used in unfocussed mode, i.e. using simply a 200-μm pinhole, on standard compounds for energy calibration of the monochromator. All energy values were measured with respect to the position of the white line (s → p transition peak) of the S K-edge spectrum of $CaSO_4$, which was assigned an energy of

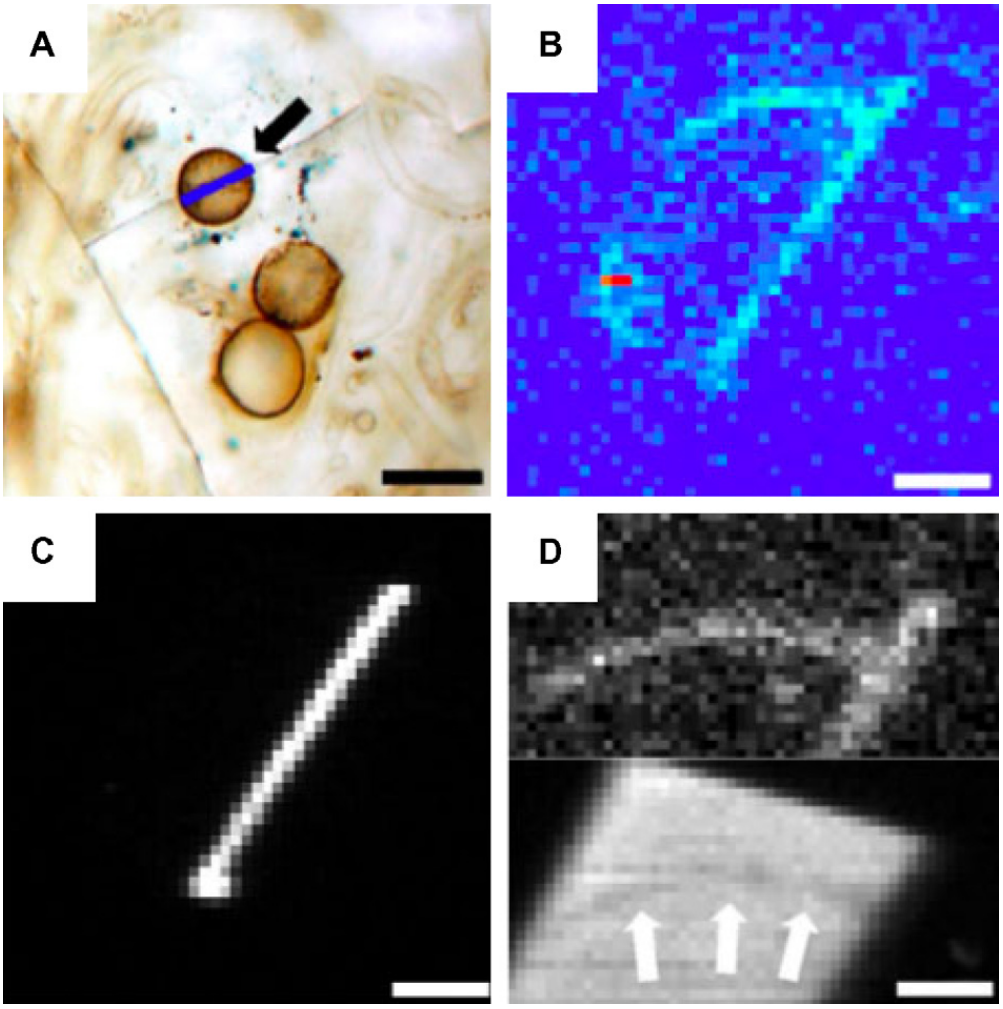

Fig. 4. A cluster of *Myxococcoides* cells in 700–800 My-old Draken conglomerate from Svalbard. (A) *Myxococcoides chlorelloidea* image with an optical microscope in transmitted light. The cell indicated by the dark arrow is 14 μm. The dark brown organic wall is readily visible; scale bar 20 μm. (B) Fluorescence map obtained at 2.5 keV of distribution of S, highlighting S-bearing carbonaceous wall. The energy peak of Pt being very close to the peak of S, the Pt coating is also visible; scale bar 5 μm. (C) Fluorescence map obtained at 2.5 keV of Pt distribution, showing thin coat of Pt on surface of section; scale bar 5 μm (D) Close-up of fluorescence map at 2.5 keV, showing S (upper) and Si distribution (lower). White arrows indicate depletion corresponding to carbonaceous wall of microfossil (scale bar 2.5 μm).

2482.5 eV. Representative S compounds (Sigma Inc.) in various oxidation states were used as standards (Table 1): inorganic sulfide (pyrite), thiol (glutathione), alkyl monosulfide (methionine), alkyl disulfide (cystine), aryl monosulfide (polyphenylene sulfide), aryl disulfide (phenylene sulfide), heterocyclic sulfide (dibenzothiophene and thianthrene) and sulfate ($CaSO_4$). Micro-XANES spectra were also collected from selected locations within the cell walls of the microfossils and on pyrite crystals within the sample. To verify that potential photoreduction effects were negligible, the final XANES spectra were obtained by summing several low integration time spectra. Each XANES spectrum was processed as follows: the spectra obtained were first corrected for I_0, the incident beam intensity before the sample. This compensates for the slow decay of the intensity of the electron beam in the storage ring and possible rapid fluctuation in intensity during spectrum acquisition. The region below the edge was fitted by a straight line which was subtracted from the spectrum to flatten and bring the baseline to zero. The spectrum was then normalized to the height of the edge jump and reported in arbitrary units.

3. Results

3.1. Fluorescence mapping

The X-ray fluorescence map of Fe at 7.2 keV shows that iron is only located within pyrite crystals (Figs. 1C and 2D), which were later identified from their micro-XANES spectra at the S K-edge,

Table 1
White line peak energy in XANES spectra of different S compounds measured at the ID21 Beamline of the European Synchrotron Radiation Facility for reduced compounds (1) or derived from the literature data (Prietzel et al., 2003) for oxidized compounds (2)

S form	Formula	Oxidation state	Compound	White line peak energy
Elemental S	S	0		
Inorganic sulphide	S_2^{2-}	−1	Pyrite	2471.9 eV (1)
Alkyl-disulfide	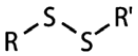	+0.2	Cystine	2472.5 eV (1)
Aryl-disulfide	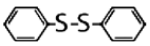	+0.2	Phenylene disulfide	2472.5 eV (1)
Thiol	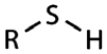	+0.5	Glutathione	2473.2 eV (1)
Alkyl-monosulfide	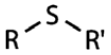	+0.5	Methionine	2473.3 eV (1)
Aryl-monosulfide		+0.5	Poly-phenylene sulfide (PPT)	2473.5 eV (1)
Thiophène	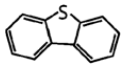	+1	Dibenzothiophene (DBT)	2473.9 eV (1)
	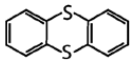	+0.5	Thianthrene	2474.3 eV (1)
Sulfoxyde	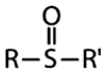	+4		2475.8 eV (2)
Sulfone	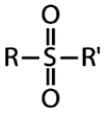	+5		2480.2 eV (2)
Sulfonate	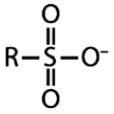	+6		2481.3 eV (2)
Sulfate	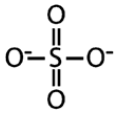	+6	$CaSO_4$	2482.5 eV (1,2)

exhibiting a white line peak at 2472 eV (Fig. 3). The pyrite crystals are commonly dispersed in the silica matrix and are also frequently closely associated with individual microfossils. However, Fe was not detected either inside the cell or in the walls, regardless of the integration time used. The X-ray fluorescence map of S at 2.5 keV over long integration times (a few seconds per pixel) on both petrographical and FIB preparations indicates that, although S is highly concentrated in pyrite, small quantities were also present in the walls of the microfossils (Figs. 1D and 2E). Since no Fe was detected in the cell walls, we conclude that the S there was not linked with Fe and therefore this element occurred in a form different from that in pyrite. The corresponding X-ray fluorescence maps of Si show depletion in the carbon rich wall of microfossils, both in the petrographical preparations and in the FIB preparations (Figs. 1B and 2F).

3.2. XANES analysis

S K-edge spectra were obtained from spot analysis of the carbonaceous walls of the microfossils (Fig. 3a). S K-edge spectra of standards are reported in Fig. 3b, the energy values of the white line peaks of the standards being reported in Table 1. The energy corresponding to the white line peak of the S compound in the cell wall presented a positive 1.9 eV difference from that of the inorganic sulfide (pyrite grain), the other form of S in the sample. Within the 0.25 eV energy resolution and after a calcite calibration, we verified that the pyrite peak energy values are identical, 2471.9 eV, in both the focussed and unfocussed experiments. Given this

calibration, the energy corresponding to the white line peak of the S compound in the cell wall is 2473.8 eV.

3.3. Quantitative analysis of S in microfossil walls

Direct empirical XRF analysis was made by comparing the same fluorescence intensity ratios for the standard and sample. For two thick multi-element samples subjected to a monochromatic incident beam of energy E_0, the ratio R can be estimated from the Sherman equation (1) (Sherman, 1954), provided only the primary absorption is taken into account and all the instrumental parameters are very close for the two samples. This ratio can thus be calculated using the following equations:

$$\begin{cases} R = \frac{c_S^{\mu F}/c_{Si}^{\mu F}}{c_S^{st}/c_{Si}^{st}} = \frac{I_S^{\mu F}/I_{Si}^{\mu F}}{I_S^{st}/I_{Si}^{st}} \times \frac{\mu_M^{\mu F}(E_{Si})/\mu_M^{\mu F}(E_S)}{\mu_M^{st}(E_{Si})/\mu_M^{st}(E_S)} \times F \\ F = \frac{\left(1+\left(\mu_M^{\mu F}(E_0)/\mu_M^{\mu F}(E_S)\right)\right)/\left(1+\left(\mu_M^{\mu F}(E_0)/\mu_M^{\mu F}(E_{Si})\right)\right)}{\left(1+\left(\mu_M^{st}(E_0)/\mu_M^{st}(E_S)\right)\right)/\left(1+\left(\mu_M^{st}(E_0)/\mu_M^{st}(E_{Si})\right)\right)} \end{cases} \quad (1)$$

where $c_i^{\mu F}$ and c_i^{st} represent the weight concentration of the element i (in this particular case, we consider the element of interest S and the main matrix component Si) analyzed from the microfossil (μF) and from the standard (st), $I_i^{\mu F}$ and I_i^{st} are the background-corrected fluorescence intensities of the element i from the sample and the standard, $\mu_M^{\mu F}(E_i)$ and $\mu_M^{st}(E_i)$ are the total mass attenuation coefficients of the matrix of the microfossil and of the reference matrix at the characteristic line energy of element i, respectively, at the incident beam energy E_0.

The most representative background-corrected fluorescence intensities for Si, $I_{Si}^{\mu F}$, and S, $I_S^{\mu F}$, emitted by the wall of one cell were determined by testing different analytical approaches (Table 2). The first two methods consist in averaging the number of photon counts recorded on n positions selected in a zone previously marked out at the μm scale. Raw accumulated counts are obtained on-line from three non-overlapping spectral regions of interest (ROIs) of 80 channels each. The ROIs for the Si and S fluorescence were centred on the characteristic Ka lines. The ROI for the background was located between the Si-ROI and S-ROI, where no elemental fluorescence was detected. The counting time, τ, is 3 s for the first method and 300 s for the second. The optimal third method for quantification of the photon counts emitted by a μm sized portion of the cell wall was achieved by analyzing the fluorescence of one unique representative spectrum with

Table 2
XRF analysis[a]

	Method 1 (τ = 3 s)						Method 2 (τ = 300 s)						Method 3 (τ^* = 300 s)				
	n	$N_{Si} \pm \sigma_{N_{Si}}$	$N_S \pm \sigma_{N_S}$	$N_{BG} \pm \sigma_{BG}$	$N_{Si}/N_S \pm \sigma_{N_{Si}/N_S}$		n	$N_{Si} \pm \sigma_{N_{Si}}$	$N_S \pm \sigma_{N_S}$	$N_{BG} \pm \sigma_{BG}$	$N_{Si}/N_S \pm \sigma_{N_{Si}/N_S}$		n	$N_{Si} \pm \sigma_{PyMCA}$	$N_S \pm \sigma_{PyMCA}$	$N_{Si}/N_S \pm \sigma_{N_{Si}/N_S}$	
SRM620	60	3466	50	5	69		14	291208	3951	305	73		20	324491	4815	67	
		(67)	(8)	(2)	(11.2)			(8031)	(100)	(23)	(3)			(569)	(78)	(1.1)	
Wall	11	5864	32	11	183		10	580756	3020	1147	192		20	582785	3139	185	
		(323)	(8)	(3)	(47)			(17690)	(1169)	(63)	(74)			(753)	(70)	(4.2)	
Matrix	9	6205	9	12	–		8	616062	586	1245	1051		20	603723	477	1265	
		(295)	(9)	(6)				(14267)	(105)	(84)	(190)			(766)	(97)	(257)	
Wall FIB-section		–	–	–	–		11	29357	498	4	59		20	44059	1336	33	
								(2861)	(165)	(2)	(21)			(267)	(40)	(1)	
Matrix FIB-section		–	–	–	–		1	31469	226	5	139		20	43522	38	1145	
								–	–	–	–			(269)	(13)	(418)	

[a] Methods #1 and #2 consist in averaging the number of counts from Si fluorescence, N_{Si}, S fluorescence, N_S and S-background, N_{BG}, measured on n positions selected on a zone previously marked out at micrometer scale. The counting time, τ, is 3 s for method 1, 300 s for method 2. The average photon counts (background corrected) are reported with the corresponding statistical variance. Method #3 is described in the text. The number of spectra, n, taken into account to calculate the average spectrum, and σ_{PyMCA} the width of the best gaussian peak fit of the fluorescence peak estimated with the PyMca software are reported for an equivalent counting time of τ^*. The error bar of N_{Si}/N_S is calculated as the variance of the Si and S fluorescence counts ratio as follows: $\sigma_{N_{Si}/N_S} = \sqrt{\frac{\sigma_{N_{Si}}^2}{N_S} + \sigma_{N_S}^2 \left(\frac{N_{Si}}{N_S^2}\right)^2}$.

the PyMCA software. Such a spectrum is calculated off line with the Artemis software by averaging spectra collected for a short counting time, τ, of 3–5 s from an area of interest selected from a recorded spectral map. In general, the two first methods are less satisfactory than the third because of the sub-μm spatial instability of the sample between the acquisition of the preliminary map and the repositioning of the beam on the wall (compare σ in Table 2). In this respect, the second approach using spectra obtained during long acquisition times is even less satisfactory than the first method. This instability leads to imprecise selection of the irradiated zone, more intense spectral variability and so to final greater variance. The minimal amount of an element, such as S, in the samples, that can be detected within a characteristic counting time for a given experimental set-up can be defined as following in the range of trace analysis (Mantler, 2006):

$$C_S^{DL} \approx \frac{3}{\beta}\sqrt{N_{BG}} \quad (2)$$

where N_{BG} is the number of the background photons in the measured total number of photons from the S-peak and β is the proportionality factor between the sum of the characteristic S-photons and the mass fraction of sulfur. The lowest detection limit for S calculated for a 3 s counting time on the SRM620 matrix is estimated to be about 10 ppm.

In order to apply the Sherman equation, the validity of the approximation of "thick samples" for the petrographical slices and the reference silica matrix was first verified. The transmission % vs. depth was calculated for the incident beam, $T_{E_i}(z)$, and for the excited fluorescence of S and Si, $T_{E_e}(z)$, with the "X-ray interaction with matter" calculator of the CXRO (Center for X-ray Optics) web site (http://www-cxro.lbl.gov/optical_constants/filter2.html) (Henke et al., 1993). We define the probed thickness of the sample, d_p, as the thickness producing more than 99% of the S-photons (or Si-photons). This thickness was then estimated as follows:

$$\frac{\int_0^{d_p} T_{E_i}(z)\cdot T_{E_e}(z)\cdot dz}{\int_0^{l} T_{E_i}(z)\cdot T_{E_e}(z)\cdot dz} \approx 99\% \quad (3)$$

where l is the depth from which less than 1‰ of the fluorescence of S escaped the sample. Distance obtained herein is overestimated, given that the reflexion geometry of the instrumental set up is not taken into account. These depths (Table 3) are inferior in all cases to the real thicknesses of the studied slices, d_s. The density and the total mass attenuation coefficients of the two studied matrices, m, deduced by fitting the transmittance vs. depth, are reported in Table 3. The combination of the fluorescence intensity ratio (Table 2) with the mass attenuation coefficient (Table 3) and the formula (1) allows estimation of the range of values of R for the wall of the microfossil at between 0.16 and 0.22. Given that the value of the ratio of the S and Si weight compositions for the reference matrix is $3.3 \pm 0.3 \times 10^{-3}$, an approximate S/Si weight ratio for the walls is estimated as 0.8×10^{-3}. The S content detected in the apparently most S-enriched cell walls is then 280 ± 45 ppm. The secondary fluorescence contribution to the Si Kα intensity, excited by an S-Kα is proportional to the Si and S concentrations. Therefore, the effective Si secondary fluorescence is higher in the reference matrix than in the microfossil matrix. In conclusion, the S content in all the imaged cellular walls must be >10 ppm (MDL) and <280 ppm.

Table 3
Macroscopic properties of the silica matrix of the microfossil and of the reference matrix (SRM620 NIST glass) required to apply formulae (1) given in the text

	Matrix of microfossil	SRM620 matrix
ρ (g cm^{-3})	2.20	2.33
d_p (μm)	10.7	11
d_s (μm)	30	3000
$\mu_M(E_0)$ (cm^2 g^{-1})	935 ± 2	860 ± 2
$\mu_M(E_{Si})$ (cm^2 g^{-1})	715 ± 2	1010 ± 2
$\mu_M(E_S)$ (cm^2 g^{-1})	1150 ± 2	1070 ± 2
$\mu_M(E_{Si})/\mu_M(E_S)$	0.622 ± 0.003	0.944 ± 0.003
c_S/c_{Si}		$3.3 \pm 0.3 \times 10^{-3}$

In comparison, the S content in the cell wall calculated using the same approach for the FIB sections is five times greater. The overestimation of the S content is consistent with the lower reabsorption of S fluorescence relative to Si in the first hundred nm below the surface. It is also consistent with a wall matrix composed of carbonaceous matter being less dense than the silica matrix. In both cases, it indicates that this particular sample preparation requires the development of a different semi-quantitative approach.

4. Discussion

4.1. Interpretation of X-ray fluorescence analysis and S K-edge XANES as S traces in parietal thiophenic compounds

This study represents the first attempt to quantify the S content of the wall of a Precambrian

microfossil. Different quantification methods were tested and it was finally established that the detectable S content varied between a minimum of 10 ppm and a maximum of 300 ppm.

The XANES study permits identification of the S observed in the wall of the microfossils as a reduced form of organic S (formal oxidation state $< +4$) that belongs, most probably, to a heterocyclic-rich type of compound such as thiophene-like compounds. The reasons are as follows. The white line peak energy of the S analyzed is 2473.8 ± 0.1 eV. It is therefore not an alkyl polysulphide (R-S_n-R, with $n > 1$) since such compounds have white line peak energy systematically less than 2472.5 eV (Chauvistré et al., 1997). Neither does it represent a thiol n or an alkyl monosulfide: the white line peak energy of glutathione and methionine studied here occur at an energy of 2473.3 ± 0.1 eV. The values reported by Sarret et al. (1999) for alkyl monosulfides vary within a 0.2 eV range, with a maximal value of 2473.4 eV recalculated according to our calibration based on the energy of the cystine peak in this study. Values reported for thiophenic compounds vary within a 0.5 eV range and have a minimal value of 2473.5 eV. The minimal energy reported for sulfoxides is 2475.6 eV (Sarret et al., 1999; Prietzel et al., 2003). The white line peak energy of the S in our study at 2473.8 ± 0.1 eV is thus significantly greater than that of alkyl sulfides (< 2473.4 eV) and less than that of sulfoxides (> 2474.6 eV). The white line peak energy at 2473.5 ± 0.1 eV of the polyphenylene standard, an aryl sulfide, suggests that the S observed in the wall of the microfossils must be enriched in thiophenic compounds, so must belong to a thiophenic or an aryl sulfide form, and thus to an organic heterocyclic-rich sulfide compound. The large, high energy edge of the main peak and the secondary peak identified in the XANES range, 2475–2480 eV, give a clear indication of the diversity of the thiophenic compounds in the cell walls. However, it is still possible that other reduced forms of sulfur, such as disulfide and alkyl/aryl sulfides, are present as minor species but in quantities below the limit of detection.

In conclusion, micro-imaging of sulfur Kα in the fossilized *Myxococcoides chlorelloidea* cells of the Draken Formation using the ID21 SXM, coupled with a first attempt at quantitative analysis of the S fluorescence and qualitative X-ray absorption near edge spectroscopy, documents the presence of organic heterocyclic-rich sulfide compounds, most probably thiophenic, in the range 10–300 ppm, in the walls of 700–800-My-old Precambrian microfossils.

4.2. Implications of sulfur SXM investigations for Draken Formation microfossils

An argument in favor of a possible endogenous origin is the low quantity of S (10–300 ppm) in the cell walls of *Myxococcoides chlorelloidea*. The reasons for this are as follows: the S content measured in the organic fractions separated from contemporary unicellular organisms is generally much lower than that in fossil OM, where the S is clearly allochthonous (cf. Introduction). For example, in recent OM, Hedges et al. (2002) estimated an organic S contents of ca. 0.5 wt% for planktonic cells, 1 wt% for certain proteins and negligible quantities for the lipid and carbohydrate components (i.e. < 500 ppm). Another study reported average elemental S concentrations of close to 4000 ppm for single marine cyanobacterial cells (Heldal et al., 2003). On the other hand, sulfur content is generally much higher (percent level) in kerogen (Tissot and Welte, 1984). Although the total amount of S in recent cells is even greater than the amount estimated for the cell walls of the *Myxococcoides chlorelloidea* microfossils studied here, the 10–300 ppm content of the microfossil is closer to that of cellular S than to typical allochthonous S.

There are two potential explanations for the presence of endogeneous sulfur in the cell walls of *Myxococcoides chlorelloidea*: either (1) it is endogenous to the cell, i.e. is related to an S-containing compound that originally formed part of the cell wall of the living microorganism, or (2) it is of biological origin but was fixed to the degraded organic molecules during early diagenesis. S of biogenic origin may have been incorporated into the cell wall of the microorganism during early diagenesis and before fossilization via the oxidative degradation of organic molecules by bacteria, coupled with the reduction of sulfate to sulfide by sulfate reducing bacteria (SRB; Summons, 1993; Kohnen et al., 1990; Wakeham et al., 1995). As there are no indications of hydrothermal activity in the environment of deposition (Knoll, 1982; Knoll et al., 1991), the presence of pyrite framboids in the silicified, microfossiliferous clasts is an additional argument in favor of the activity of SRB in the anoxic layers of the shallow water sediment. Even though the shallow water sediment and its biota were rapidly

silicified, the presence of numerous pyrite crystals clearly indicates that silicification took place after the early diagenetic precipitation of pyrite.

Although the above arguments, based primarily on the SXM analysis, weigh in favor of an endogenous, organic origin for the S and the thiophenic compounds, we cannot completely exclude a possibility of an as yet unidentified (non-hydrothermal) abiotic sulfurization process for the organic parietal compounds. Neither is it possible to exclude a possible formation of thiophenic compounds during diagenesis, for example by the aromatization of initial parietal non-thiophenic organics, as demonstrated in the laboratory with thermal treatment experiments (Sarret et al., 2002). It will be necessary to make complementary analyses, discussed below, to arrive at a conclusive explanation.

4.3. Implications and perspectives for Precambrian microfossil studies

SXM investigations at the sulfur K-edge such as the one developed in this study present numerous advantages for Precambrian microfossil studies. They permit the fast and non-destructive selection of organically well-preserved, individual microfossils from within a population, especially those with cell walls characterized by low S content indicating sulfur of endogeneous origin. By restricting the number of samples of interest, such quantitative XRF imaging coupled to XANES microspectrometry at the sulfur K-edge increases and accelerates significantly the potential of finding important biomarkers and of better understanding the origin of the organic S compounds.

Minimum detection limits for sulfur Kα with SRXRF are better than those obtained using electron probe microanalysis (EPMA) of sulfur in fossilized carbonaceous cells (Boyce et al., 2001). Moreover, although minimum EPMA detection levels as low as 6–8 ppm for Kα peaks of transition metals of the first row were estimated by Fialin et al. (1999), the experimental conditions used (total counting time 15 min with a beam of 35 kV and 500 nA on standards but with a beam-excited area of 80 μm^2) are not relevant to the analysis of the kinds of microstructures investigated in this study. Thus EPMA is not suitable at present for detecting traces of S in the 10–100 ppm range in our microfossils. Apart from the advantage of the detection limit with high spatial resolution, the hard X-rays can penetrate to greater depth than possible with EPMA (several μm as opposed to < 1 μm), thereby enabling observation of micron-sized structures embedded a few microns below the surface. Nor is it necessary to coat surfaces with a conductive layer. Another clear advantage of SXM is its combination with XANES, which permits chemical speciation studies. Although sulfur L edge is more efficient than S K-edge XANES for overcoming uncertainty in the determination of the reduced forms of S (Sarret et al., 1999), the former technique requires considerable sample preparation (with the production of ultra-thin slices < 800 nm for imaging purposes and < 400 nm for quantitative spectroscopy; Cody et al., 1996). With respect to the study of fossilized cells, sulfur L edge analysis requires preparation of ultra-thin sections of 100–200 by ultra-microtoming (Boyce et al., 2002) and their demineralisation (Boyce et al., 2003). Likewise, although carbon K-edge XANES has been successfully used to study organic compounds (Cody et al., 1996), this also requires the preparation of ultra-thin sections. In contrast, S K-edge XANES is rapid and can be undertaken directly on petrological 30 μm thick surfaces without further painstaking preparation.

In comparison to Nano-SIMS (Robert et al., 2005; Oehler et al., 2006), the spatial resolution of SXM is comparable. However, Nano-SIMS cannot provide either a quantitative elemental map or molecular information. On the other hand, complementary in situ C and S isotope measurements made on a cellular scale (e.g., Kakegawa and Nanri, 2006; House et al., 2000) would be a useful method for studying microfossils enriched in S organic compounds. In this way, it should be possible to investigate the origin and diagenetic transformations of well-preserved Precambrian organic compounds. Such investigations are envisaged for this sample.

Our investigation opens up important perspectives for Precambrian microfossil studies in general. For instance, further studies using the quantification procedure employed and aimed at the precise measurement of sulfur in the numerous taxa preserved in the Draken Formation (Knoll, 1982; Knoll et al., 1991) can potentially reveal interesting information concerning the taxonomic and taphonomic history of this fossiliferous assemblage. As an example, it would be interesting to look for S in other microfossils from the Draken Formation, such as the filamentous *Siphonophycus* (Knoll et al., 1991). It is commonly accepted that these filaments are the remnants of the sheaths of ancient cyanobacteria. Having a polysaccharide composi-

tion, the sheaths of these filaments may be different, from a chemical point of view, from the wall of *Myxococcoides chlorelloidea*. It is possible that this difference, especially the relative quantity of carbon double bonds, can be expressed in terms of difference in the concentration of S integrated into the kerogenous wall. In given cases where an allochthonous S source can be excluded, the identification and quantification of specific S species in carbonaceous microfossils is a very useful biogenicity indicator. Our study also shows that SXM could possibly become an important instrument in the study of older, more controversial carbonaceous Archaean microstructures (e.g. Schopf, 1993; Brasier et al., 2002; Schopf et al., 2002; Westall et al., 2006b) that are several billion years older than the well preserved Neoproterozoic microfossils of clear biogenic origin investigated here.

5. Conclusions

Being element-specific, non-destructive, sensitive to oxidation state and applicable to small individual microfossils without any coating, micro-XRF imaging and micro-XANES analysis using scanning X-ray microscopy (SXM) are efficient techniques for the in situ mapping and determination of sulfur content and species in Precambrian microfossils. The techniques have demonstrated the presence of trace amounts of sulfur, mainly in the form of heterocyclic organic sulfur compounds, in the carbonaceous walls of 700–800-My-old *Myxococcoides chlorelloidea* cells of the Draken Formation. The sulfur is most likely endogenous in origin, although it is not possible to determine whether it is directly related to specific S-rich cell components and/or whether it was incorporated through early diagenesis. The presence of sulfur indicates that the organic matter in these microfossils is relatively well preserved (offering potential for the preservation of molecular biomarkers).

The study opens up perspectives for Precambrian microfossil studies in general. Quantitative analysis of organic sulfur can be used as an indicator of biogenicity and can provide information regarding the taxonomic and taphonomic history of microfossils.

Acknowledgements

We gratefully acknowledge Professor Andrew Knoll for providing the samples, Annie Richard and Jean-Gabriel Breheret for SEM imaging, Maggy Colas for Raman analysis and the CP2M team for FIB, STEM and HRTEM work. We acknowledge the European Synchrotron Radiation Facility for provision of synchrotron radiation and Jean Susini of the ID21 beamline. Gordon Southam is kindly thanked for critical comments, as are P.F. Greenwood and an anonymous reviewer. The work was supported by CNES, Région Centre, ANR and the CNRS.

Associate Editor—**L. Schwark**

References

Acholla, F.V., Orr, W.L., 1993. Pyrite removal from kerogen without altering organic matter: the chromous chloride. Energy and Fuels 7, 406–410.

Arouri, K., Greenwood, P.F., Walter, M.R., 2000. Biological affinities of Neoproterozoic acritarchs from Australia: microscopic and chemical characterization. Organic Geochemistry 31, 75–89.

Boyce, C.K., Hazen, R.M., Knoll, A.H., 2001. Nondestructive, *in situ*, cellular-scale mapping of elemental abundances including organic carbon in permineralized fossils. Proceedings of the National Academy of Sciences of the USA 98, 5970–5974.

Boyce, C.K., Cody, G.D., Feser, M., Jacobsen, C., Knoll, A.H., Wirick, S., 2002. Organic chemical differentiation within fossil plant cell walls detected with X-ray spectromicroscopy. Geology 30, 1039–1042.

Boyce, C.K., Cody, G.D., Fogel, M.L., Hazen, R.M., Alexander, C.M. O'D, Knoll, A.H., 2003. Chemical evidence for cell wall lignification and the evolution of tracheids in Early Devonian Plants. International Journal of Plant Science 164, 691–702.

Brasier, M.D., Green, O.R., Jephcoat, A.P., Kleppe, A.K., Van Kranendonk, M.J., Lindsay, J.F., Steele, A., Grassineau, N.V., 2002. Questioning the evidence for Earth's oldest fossils. Nature 416, 76–81.

Buick, R., 1990. Microfossil recognition in Archean rocks: an appraisal of spheroids and filaments from a 3500 M.Y. old chert-barite unit at North Pole, Western Australia. Palaios 5, 441–459.

Chauvistré, R., Hormes, J., Hartmann, E., Etzenbach, N., Hosch, R., Hahn, J., 1997. Sulphur K-shell absorption spectroscopy of the sulfanes R-S_n-R, $n = 2$–4. Chemical Physics 223, 293–302.

Cody, G.D., Botto, R.E., Ade, H., Wirick, S., 1996. The application of soft X-ray microscopy to the *in situ* analysis of sporinite in Coal. International Journal of Coal Geology 32, 69–86.

Durand, B., Monin, J.C., 1980. Elemental analysis of kerogens (C, H, O, N, S, Fe). In: Durand, B. (Ed.), Kerogen, Insoluble Organic Matter from Sedimentary Rocks. Technip, Paris, pp. 113–142.

Fialin, M., Rémy, H., Richard, C., Wagner, C., 1999. Trace element analysis with the electron microprobe: new data and perspectives. American Mineralogist 84, 70–77.

Foriel, J., Philippot, P., Susini, J., Dumas, P., Somogy, A., Salome, M., Khodja, H., Menez, B., Fouquet, Y., Moreira, Y., Lopez-Garcia, P.P., 2004. High-resolution imaging of sulphur oxidation states, trace elements and organic molecules distribution in individual microfossils and contemporary microbial filaments. Geochimica et Cosmochimica Acta 68, 1561–1569.

Fleet, M.E., 2005. XANES Spectroscopy of sulfur in Earth Materials. The Canadian Mineralogist 43, 1811–1838.

Hedges, J.I., Baldock, J.A., Gelinas, Y., Lee, C., Peterson, M.L., Wakeham, S.G., 2002. The biochemical and elemental compositions of marine plankton: a NMR perspective. Marine Chemistry 78, 47–63.

Heldal, M., Scanlan, D.L., Norland, S., Thingstad, F., Mann, N.H., 2003. Elemental composition of single cells of various strains of marine Prochlorococcus and Synechococcus using X-ray microanalysis. Limnology and Oceanography 48, 1732–1743.

Henke, B.L., Gullikson, E.M., Davis, J.C., 1993. X-ray interactions: photoabsorption, scattering, transmission, and reflection at $E = 50$–30000 eV, $Z = 1$–92. Atomic Data and Nuclear Data Tables 54, 181–342.

House, C.H., Schopf, J.W., McKeegan, K.D., Coath, C.D., Harrison, T.M., Stetter, K.O., 2000. Carbon isotopic composition of individual Precambrian microfossils. Geology 28, 707–710.

Kakegawa, T., Nanri, H., 2006. Sulphur and carbon isotope analyses of 2.7 Ga stromatolites, cherts and sandstones in Jeerinah formation, Western Australia. Precambrian Research 148, 115–124.

Kelemen, S.R., Afeworki, A.M., Gorbaty, M.L., Sansone, M., Kwiatek, P.J., Walters, C.C., Freund, H., Siskin, M., Bence, A.E., Curry, D.J., Solum, M., Pugmire, R.J., Vandenbroucke, M., Leblond, M., Behar, F., 2007. Direct characterization of kerogen by X-ray and solid state nuclear magnetic resonance methods. Energy and fuels 21, 1548–1561.

Knoll, A.H., 1982. Microfossils from the late Precambrian Draken Conglomerate, Ny Friesland, Svalbard. Journal of Paleontology 56, 755–790.

Knoll, A., 2003. Life on a young planet: the first three billion years of evolution on earth. Princeton University Press, New Jersey.

Knoll, A.H., Swett, K., Mark, J., 1991. Paleobiology of a Neoproterozoic tidal flat/lagoonal complex: the Draken Conglomerate Formation, Spitsbergen. Journal of Paleontology 65, 531–570.

Kohnen, M.E.L., Sinninghe Damsté, J.S., Kock-van Dalen, A.C., ten Haven, H.L., Rullkötter, J., de Leeuw, J.W., 1990. Origin and diagenetic transformations of C_{25} and C_{30} highly branched isoprenoid S compounds: further evidence for the transformation of organically bound S during early diagenesis. Geochimica et Cosmochimica Acta 54, 3053–3063.

Labrot, P., 2006. Microscopie à force atomique de microfossiles Precambriens. PhD thesis, University of Orléans.

Lemelle, L., Simionovici, A., Susini, J., Oger, P., Chukalina, M., Rau, C., Golosio, B., Gillet, P., 2003. X-ray imaging techniques and exobiology. Journal de Physique IV 104, 377–380.

Lemelle, L., Salome, M., Fialin, M., Simionovici, A., Gillet, P., 2004. In situ identification and X-ray imaging of microorganisms distribution on the Tatahouine meteorite. Spectrochimica Acta 59, 1703–1710.

Mantler, M., 2006. Errors and reliability in quantitative analysis. In: Beckhoff, B., Kanngiesser, B., Langhoff, N., Wedell, R., Wolff, H. (Eds.), Handbook of Practical X-Ray Fluorescence Analysis. Springer, Heidelberg, pp. 309–407.

Marshall, C.P., Javaux, E.J., Knoll, A.H., Walter, M.R., 2005. Combined micro-Fourier transform infrared (FTIR) spectroscopy and micro-Raman spectroscopy of Proterozoic acritarchs: a new approach to Palaeobiology. Precambrian Research 138, 208–224.

Oehler, D.Z., Robert, F., Mostefaoui, S., Meibom, A., Selo, M., McKay, D., 2006. Chemical mapping of Proterozoic organic matter at submicron spatial resolution. Astrobiology 6, 838–850.

Pickering, I.J., Prince, R.C., Divers, T., George, G.N., 1998. Sulphur K-edge X-ray absorption spectroscopy for determining the chemical speciation of sulphur in biological systems. Federation of European Biochemical Societies Letters 441, 11–14.

Prietzel, J., Thieme, J., Neuhäusler, U., Susini, J., Kögel-Knabner, I., 2003. Speciation of S in soils and soil particles by X-ray spectromicroscopy. European Journal of Soil Science 54, 423–433.

Robert, F., Selo, M., Hillion, F., Skrzypczak, A., 2005. Nanosims images of Precambrian fossil cells. Abstract, Lunar and Planetary Science XXXVI.

Rompel, A., Cinco, R.M., Latimer, M.J., McDermott, A.E., Guiles, R.D., Quintanilha, A., Krauss, R.M., Sauer, K., Yachandra, V.K., Klein, M.P., 1998. Sulfur K-edge X-ray absorption spectroscopy: a spectroscopic tool to examine the redox state of S-containing metabolites in vivo. Proceedings of the National Academy of Sciences USA 95, 6122–6127.

Sarret, G., Connan, J., Kasrai, M., Bancroft, G.M., Charrié-Duhaut, A., Lemoine, S., Adam, P., Albrecht, P., Eybert-Bérard, L., 1999. Chemical forms of sulphur in geological and archeological asphaltenes from Middle East, France and Spain determined by sulphur K-and L-edge X-ray absorption near-edge structure spectroscopy. Geochimica et Cosmochimica Acta 63, 3767–3779.

Sarret, G., Mongenot, T., Connan, J., Derenne, S., Kasrai, M., Bancroft, G.M., Largeau, C., 2002. Sulphur speciation in kerogens of the Orbagnoux deposit (Upper kimmeridgian, Jura) by XANES spectroscopy and pyrolysis. Organic Geochemistry 33, 877–895.

Schopf, J.W., 1993. Microfossils of the Early Archean Apex chert: new evidence of the antiquity of life. Nature 260, 640–646.

Schopf, J.W., Kudryavtsev, A.B., Agresti, D.G., Wdowiak, T.J., Czaja, A.D., 2002. Laser-Raman imagery of Earth's earliest fossils. Nature 416, 73–76.

Sherman, J., 1954. ASTM Special Technical Publication No. 157, p. 27.

Summons, R.E., 1993. A review of fundamental aspects of organic matter formation, preservation and composition. In: Engel, M.A., Macko, S.A. (Eds.), Organic Geochemistry, Principles and Applications. Plenum Press, New York, pp. 3–21.

Susini, J., Salome, M., Fayard, B., Ortega, R., Kaulich, B., 2002. The scanning X-ray microprobe at the ESRF by X-ray microscopy beamline. Surface Review and Letters 9, 203–211.

Tissot, B.P., Welte, D.H., 1984. Petroleum Formation and Occurrence, 2nd ed. Springer, Heidelberg.

Wakeham, S.G., Sinninghe Damsté, J.S., Kohnen, M.E.L., de Leeuw, J.W., 1995. Organic sulphur compounds formed

during early diagenesis in Black Sea sediments. Geochimica et Cosmochimica Acta 59, 521–533.

Westall, F., 1997. The influence of cell wall composition on the fossilisation of bacteria and the implications for the search for early life forms. In: Cosmovici, C.B., Bowyer, S., Werthimer, D. (Eds.), Astronomical and Biochemical Origins and the Search for Life in the Universe. Editrici Compositori, Bologna, pp. 491–504.

Westall, F., de Vries, S.T., Nijman, W., Rouchon, V., Orberger, B., Pearson, V., Watson, J., Verchovsky, A., Wright, I., Rouzaud, Marchesini, D., Anne, S., 2006b. The 3.466 Ga Kitty's Gap Chert, an Early Archaean microbial ecosystem. In: Reimold, W.U., Gibson, R. (Eds.), Processes on the Early Earth, vol. 405. Geological Society of America Special Publication, pp. 105–131.

Whelan, J.K., Thompson-Rizer, C.L., 1993. Chemical methods for assessing kerogen and protokerogen types and maturity. In: Engel, M.A., Macko, S.A. (Eds.), Organic Geochemistry, Principles and Applications, vol. 861. Plenum Press, New York, pp. 289–353.